Derivative sources in lattice spectroscopy of excited light-quark mesons

Christof Gattringer,[*] Leonid Ya. Glozman,[+] C. B. Lang,[‡] and Daniel Mohler[§]
Institut für Physik, Unversität Graz, 8010 Graz, Austria

Sasa Prelovsek[‖]
Department of Physics, University of Ljubljana and Institut Joszef Stefan, 1001 Ljubljana, Slovenia
(Received 3 March 2008; published 8 August 2008)

We construct efficient interpolating fields for lattice spectroscopy of mesons by applying covariant derivatives on Jacobi-smeared quark sources. These interpolators are tested in a quenched calculation of excited mesons based on the variational method. We present results for pseudoscalar, scalar, vector and pseudovector mesons.

DOI: 10.1103/PhysRevD.78.034501 PACS numbers: 11.15.Ha, 12.38.Gc

I. INTRODUCTION

A clean extraction of excited hadron masses from a lattice QCD simulation is a serious challenge. However, an *ab initio* determination of properties for excited light hadrons would provide highly interesting information on the chiral dynamics of QCD.

Excited hadrons are rather nontrivial objects to study on the lattice. One of the main reasons for difficulties is the fact that excited states appear only as subleading contributions in Euclidean two-point functions. Although a variety of other approaches has been tried, including Bayesian methods [1–3], an NMR-inspired blackbox method [4,5] and evolutionary fitting techniques [6], the most powerful method is probably the variational approach [7,8]. The reason for its power is the fact that in the variational method not only a single correlator is studied, but a whole matrix of correlation functions. Consequently more information is extracted from the system.

The successful implementation of the variational method hinges crucially on the set of basis interpolators that are used in the correlation matrix. A particularly important criterion is that the interpolators have a large overlap with the physical states in a given channel, i.e., with both ground and excited states. In this article we build on earlier work [9–12], where Jacobi-smeared quark sources with different width were used to construct hadron interpolators that allow for nodes in their radial wave function. To construct a richer set of interpolators, we now also include derivative sources for light-quark spectroscopy.

Interpolators with derivatives have been widely used for heavy-quark systems (see, for example, [13–15]). They have also been applied by Burch *et al.* [16,17] for light mesons and by Lacock *et al.* [18] to the study of both orbital excitations of mesons and hybrids. Note that the approach in [18] differs from ours. In [18] the interpolators are built with quarks displaced relative to each other connected by certain paths which are classified with respect to irreducible representations of the symmetry group of the hypercubic lattice. That approach is similar to the one adopted by Basak *et al.* [19–22] for baryons.

In our paper we test derivative sources in a quenched excited meson spectroscopy calculation. In particular we study the pseudoscalar, scalar, vector and pseudovector channels. Depending on the channel we find considerable improvement of the signal for some of the excited and ground states. Preliminary results with our derivative sources were already reported in [23–25].

II. SETTING OF THE CALCULATION

A. Variational method

The central idea of the variational method [7,8] is to use several different interpolators O_i, $i = 1, \ldots N$ with the quantum numbers of the desired state and to compute all cross correlators for interpolators projected to fixed spatial momentum (zero in this work),

$$C(t)_{ij} = \langle O_i(t) O_j^\dagger(0) \rangle. \tag{1}$$

In Hilbert space these correlators have the decomposition

$$C(t)_{ij} = \sum_n \langle 0|O_i|n\rangle\langle n|O_j^\dagger|0\rangle e^{-tM_n}. \tag{2}$$

Using the factorization of the amplitudes one can show [8] that the eigenvalues $\lambda_k(t)$ of the generalized eigenvalue problem,

$$C(t)\vec{v}_k = \lambda_k(t) C(t_0)\vec{v}_k, \tag{3}$$

behave as

$$\lambda_k(t) \propto e^{-tM_k}[1 + \mathcal{O}(e^{-t\Delta M_k})], \tag{4}$$

where M_k is the mass of the kth state and ΔM_k is the difference to neighboring states. In Eq. (3) the eigenvalue problem is normalized at a time slice $t_0 \leq t$.

[*]christof.gattringer@uni-graz.at
[+]leonid.glozman@uni-graz.at
[‡]christian.lang@uni-graz.at
[§]Corresponding author.
daniel.mohler@uni-graz.at
[‖]sasa.prelovsek@ijs.si

Equation (4) shows that each eigenvalue predominantly decays with a single mass: The largest eigenvalue decays with the mass of the ground state, the second largest eigenvalue with the mass of the first excited state, and so on. Thus, the variational method disentangles the signals of the ground and excited states. As a consequence simple, stable two-parameter fits become possible.

At this point we remark that the variational method also treats ghost contributions correctly, which in some channels show up in a quenched or partially quenched calculation at small quark masses [26]. It was shown in [27] that in the variational approach the ghost contribution couples to an individual eigenvalue (up to the correction term) in the same way as a proper physical state. Thus, ghost contributions are disentangled from the physical states and need not be modeled in the further analysis of the exponential decay of the eigenvalues.

To visualize the results and to determine possible fit ranges, we plot effective masses which are built from the ratios of eigenvalues

$$aM_{k,\mathrm{eff}}\left(t+\frac{1}{2}\right)=\ln\left(\frac{\lambda_k(t)}{\lambda_k(t+1)}\right). \tag{5}$$

For those values of t where the exponential decay of the eigenvalue is governed by a single state, the effective masses form pronounced plateaus.

It is an interesting observation that for the same values of t, where the effective mass plateaus form, also the corresponding eigenvectors are approximately constant as a function of t. An example of this behavior is given in Fig. 5 (discussed later), where we show the entries of the eigenvectors for the three largest eigenvalues as a function of t. This time independence of the eigenvectors serves as a ''fingerprint'' for the physical states. To be more precise, the eigenvectors we use for such fingerprints are the eigenvectors of the regular eigenvalue problem

$$C(t_0)^{-(1/2)}C(t)C(t_0)^{-(1/2)}\vec{v}'_k=\lambda_k(t)\vec{v}'_k, \tag{6}$$

which obviously has the same eigenvalues $\lambda_k(t)$ as the problem (3), but gives rise to orthogonal eigenvectors $\vec{v}'_k$.

In our analysis we only fit states which give rise to a plateau in both the effective mass and the corresponding eigenvector. Ideally, t_0 should be chosen large. However, large t_0 also tends to increase the statistical noise. We explored the dependence of the effective mass plateaus on the time slice t_0 and usually found the best results for $t_0=1$. So unless noted otherwise, t_0 will be fixed to $t_0=1$ for all results quoted (our sources are located at $t=0$; see next section).

B. Smeared sources and sinks

In order to optimize the overlap with the ground and first few excited states, one commonly uses quark smearing. We first construct extended sources by the Jacobi smearing [28,29] of point sources S_0 located at time slice $t=0$:

$$S_0^{(\alpha,a)}(\vec{y},t)_{\rho,c}=\delta(\vec{y},\vec{0})\delta(t,0)\delta_{\rho\alpha}\delta_{ca}, \tag{7}$$

$$S^{(\alpha,a)}=\sum_{n=0}^{N}\kappa^n H^n S_0^{(\alpha,a)}, \tag{8}$$

$$H(\vec{x},\vec{y})=\sum_{i=1}^{3}(U_i(\vec{x},0)\delta(\vec{x}+\hat{i},\vec{y}) + U_i(\vec{x}-\hat{i},0)^\dagger\delta(\vec{x}-\hat{i},\vec{y})). \tag{9}$$

The smearing has two parameters κ and N and leads to gauge covariant, approximately Gaussian shaped sources of different width. We use the same combinations of parameters as in [9] and we refer to our sources as ''narrow'' (S_n) and ''wide'' (S_w).

Our derivative quark sources W_{∂_i} are constructed by applying a covariant derivative to the wide sources:

$$P_i(\vec{x},\vec{y})=U_i(\vec{x},0)\delta(\vec{x}+\hat{i},\vec{y})-U_i(\vec{x}-\hat{i},0)^\dagger\delta(\vec{x}-\hat{i},\vec{y}), \tag{10}$$

$$W_{\partial_i}=P_iS_w. \tag{11}$$

These sources are then used in the construction of meson interpolators of definite quantum numbers.

C. Meson interpolators

Table I shows our interpolators for the different meson channels considered. In the first column the interpolators are numbered according to their structure rather than consecutively. Numbers 1–6 denote the Jacobi-smeared interpolators of [9], while the interpolators 7–12 contain at least one derivative. Notice also that only the combination of number and quantum numbers uniquely labels an interpolator.

In some cases, an (anti-) symmetrization of the interpolators is necessary to obtain the correct behavior under charge conjugation. Therefore, interpolators denoted as $\bar{u}_{\partial_i}\Gamma d_{n/w}$ in Table I should be read as $\bar{u}_{\partial_i}\Gamma d_{n/w}-\bar{u}_{n/w}\Gamma d_{\partial_i}$. We restrict ourselves to light, isovector ($I=1$) mesons with degenerate quark masses $m_u=m_d$.

All interpolators have been classified by their continuum quantum numbers IJ^{PC}, both for nonvanishing quark mass and in the chiral limit. As usual, P is the spatial parity, J is the total spin, and I the isospin. For a neutral $q\bar{q}$ system [30] the C parity is related to the other quantum numbers in a standard way. To simplify the notation, we omit the spin and isospin projections in the notation.

In addition to the quantum numbers listed in Table I, the lattice interpolators will also couple to continuum states with higher J due to the loss of rotational symmetry [14,18]. The lattice interpolators for 0^{PC} mesons couple also to $J\geq 4$, but this does not influence our conclusions since there are no observed resonances with $J\geq 4$ in the energy regime of interest. The lattice interpolators for 1^{PC} mesons couple also to $J\geq 3$ and the issue is discussed in Sec. III C.

TABLE I. List of our meson interpolators. The numbers in the first column together with the quantum numbers IJ^{PC} given in the third column label the interpolators uniquely. The fourth and fifth column specify the chiral representation and the coupling in the chiral limit. The lattice interpolators may also couple to states with higher angular momentum J [14,18]. The subscripts n and w refer to narrow and wide smearing of u and d quarks. The subscript ∂_i denotes derivative smearing in i direction. Where it appears, the index i is summed over the spatial directions 1,2,3. The time direction is 4 and the corresponding Dirac matrix is γ_4. For the vector and pseudovector channels the index k (not summed !) can have values $k = 1, 2, 3$.

Number	Operator	IJ^{PC} beyond chiral limit	Chiral representation	IJ^{PC} chiral limit	Comment
1	$\bar{u}_n d_n$	$1\,0^{++}$	$(\frac{1}{2},\frac{1}{2})_b$	$1\,0^{++}$	
2	$\bar{u}_n d_w$				
3	$\bar{u}_w d_w$				
7	$\bar{u}_{\partial_i}\gamma_i d_n$	$1\,0^{++}$	$(1,0)\oplus(0,1)$	does not exist (only $J \geq 1$)	not coupling to scalar in the chiral limit
8	$\bar{u}_{\partial_i}\gamma_i d_w$				
9	$\bar{u}_{\partial_i}\gamma_i\gamma_4 d_n$	$1\,0^{++}$	$(\frac{1}{2},\frac{1}{2})_b$	$1\,0^{++}$	
10	$\bar{u}_{\partial_i}\gamma_i\gamma_4 d_w$				
11	$\bar{u}_{\partial_i} d_{\partial_i}$	$1\,0^{++}$	$(\frac{1}{2},\frac{1}{2})_b$	$1\,0^{++}$	
1	$\bar{u}_n\gamma_5 d_n$	$1\,0^{-+}$	$(\frac{1}{2},\frac{1}{2})_a$	$1\,0^{-+}$	
2	$\bar{u}_n\gamma_5 d_w$				
3	$\bar{u}_w\gamma_5 d_w$				
4	$\bar{u}_n\gamma_4\gamma_5 d_n$	$1\,0^{-+}$	$(1,0)\oplus(0,1)$	does not exist (only $J \geq 1$)	time component of axial vector coupling due to chiral symmetry breaking
5	$\bar{u}_n\gamma_4\gamma_5 d_w$				
6	$\bar{u}_w\gamma_4\gamma_5 d_w$				
9	$\bar{u}_{\partial_i}\gamma_i\gamma_4\gamma_5 d_n$	$1\,0^{-+}$	$(\frac{1}{2},\frac{1}{2})_a$	$1\,0^{-+}$	
10	$\bar{u}_{\partial_i}\gamma_i\gamma_4\gamma_5 d_w$				
11	$\bar{u}_{\partial_i}\gamma_5 d_{\partial_i}$	$1\,0^{-+}$	$(\frac{1}{2},\frac{1}{2})_a$	$1\,0^{-+}$	
12	$\bar{u}_{\partial_i}\gamma_4\gamma_5 d_{\partial_i}$	$1\,0^{-+}$	$(1,0)\oplus(0,1)$	does not exist (only $J \geq 1$)	time component of axial vector coupling due to chiral symmetry breaking
1	$\bar{u}_n\gamma_k d_n$	$1\,1^{--}$	$(1,0)\oplus(0,1)$	$1\,1^{--}$	
2	$\bar{u}_n\gamma_k d_w$				
3	$\bar{u}_w\gamma_k d_w$				
4	$\bar{u}_n\gamma_k\gamma_4 d_n$	$1\,1^{--}$	$(\frac{1}{2},\frac{1}{2})_b$	$1\,1^{--}$	
5	$\bar{u}_n\gamma_k\gamma_4 d_w$				
6	$\bar{u}_w\gamma_k\gamma_4 d_w$				
7	$\bar{u}_{\partial_k} d_n$	$1\,1^{--}$	$(\frac{1}{2},\frac{1}{2})_b$	$1\,1^{--}$	
8	$\bar{u}_{\partial_k} d_w$				
11	$\bar{u}_{\partial_i}\gamma_k d_{\partial_i}$	$1\,1^{--}$	$(1,0)\oplus(0,1)$	$1\,1^{--}$	
1	$\bar{u}_n\gamma_k\gamma_5 d_n$	$1\,1^{++}$	$(1,0)\oplus(0,1)$	$1\,1^{++}$	
2	$\bar{u}_n\gamma_k\gamma_5 d_w$				
3	$\bar{u}_w\gamma_k\gamma_5 d_w$				
11	$\bar{u}_{\partial_i}\gamma_k\gamma_5 d_{\partial_i}$	$1\,1^{++}$	$(1,0)\oplus(0,1)$	$1\,1^{++}$	

In the chiral limit, the different interpolators listed in Table I can be classified into representations of chiral $SU(2)_L \times SU(2)_R$ and $U(1)_A$ groups [31,32], as well as with respect to their partial wave $^{2S+1}L_J$ decomposition [33]. Below we review these properties.

We label with R the index of the chiral representation; $R = (0,0)$, $(1/2,1/2)_a$, $(1/2,1/2)_b$, or $(0,1)\oplus(1,0)$. The chiral basis $\{R; IJ^{PC}\}$ is obviously consistent with Poincaré invariance. Each of the interpolators in Table I has a fixed $U(1)_A$ transformation property. Namely, all those interpo-

lators that belong to $(0,0)$ or $(0,1)\oplus(1,0)$ of $SU(2)_L \times SU(2)_R$ are scalars with respect to $U(1)_A$, i.e., they transform into themselves under a $U(1)_A$ transformation. However, interpolators with opposite spatial parity and the same spin J and isospin I from the distinct $(1/2,1/2)_a$ and $(1/2,1/2)_b$ representations of $SU(2)_L \times SU(2)_R$ transform into each other upon $U(1)_A$.

The set of quantum numbers $\{R; IJ^{PC}\}$ uniquely fixes a partial wave content $|I;{}^{2S+1}L_J\rangle$ of the quark-antiquark system in the center-of-mass frame [33]. In particular, the different interpolators from Table I with quantum numbers $1\,0^{++}$ belonging to $(1/2,1/2)_b$ represent the $|1;{}^3P_0\rangle$ partial wave in the $\bar{q}q$ system, irrespective of the number of derivatives in the interpolator. Note however that there are some interpolators in the $1\,0^{++}$ channel (numbers 7 and 8) which will not couple to the scalars in the chiral limit, since they belong to the $(0,1)\oplus(1,0)$ representation which requires $J \geq 1$.

For the $1\,0^{-+}$ sector, there are two types of interpolators: interpolators (1–3, 9–10, 11) which transform as $(1/2,1/2)_a$ and represent the $|1;{}^1S_0\rangle$ partial wave, and time components of pseudovector interpolators which couple to pseudoscalars due to partial conservation of the axial vector current and which belong to the $(0,1)\oplus(1,0)$ representation.

In the $1\,1^{++}$ sector, all interpolators transform as $(0,1)\oplus(1,0)$ and couple only to the $|1;{}^3P_1\rangle$ partial wave. However, there are two kinds of interpolators with quantum numbers $1\,1^{--}$. They are the *fixed* and orthogonal superpositions of two different partial waves:

$$|(0,1)+(1,0);1\,1^{--}\rangle = \sqrt{\tfrac{2}{3}}|1;{}^3S_1\rangle + \sqrt{\tfrac{1}{3}}|1;{}^3D_1\rangle,$$
$$|(1/2,1/2)_b;1\,1^{--}\rangle = \sqrt{\tfrac{1}{3}}|1;{}^3S_1\rangle - \sqrt{\tfrac{2}{3}}|1;{}^3D_1\rangle.$$

The interpolators 1–3 and 11 from Table I belong to the $|(0,1)+(1,0);1\,1^{--}\rangle$ representation, while all others transform as $|(1/2,1/2)_b;1\,1^{--}\rangle$.

D. Technicalities

For our analysis we used 99 uncorrelated quenched gauge configurations generated with the Lüscher-Weisz gauge action [34,35]. We work on a $16^3\times 32$ lattice with $a = 0.148$ fm determined [36] from the Sommer parameter (using $r_0 = 0.5$ fm). For comparison we also use old data from a $20^3\times 32$ lattice at $a = 0.119$ fm, where, however, only the Jacobi-smeared sources without additional derivatives are available. The boundary conditions for the gauge fields are periodic in all four directions. The quark propagators were computed from the Chirally Improved Dirac operator [37,38] with periodic boundary conditions in space and antiperiodic boundary conditions in the time coordinate. We study several quark mass parameters in the range $am_q = 0.02\ldots0.2$. We fold individual entries of the correlation matrix resulting from propagation in positive and negative time direction according to their symmetry, which reduces the statistical errors and improves the quality of the data significantly. Unless noted otherwise, the errors we quote are statistical errors determined with the jackknife method.

Where possible we also indicate the systematical uncertainties by a shaded band (Figs. 3 and 4 etc.). The upper and lower limits of this band are obtained by repeating the fits of the eigenvalues using different fit ranges and varying the interpolators used in the correlation matrix. Although this is certainly only a rough estimate of the systematic uncertainty in the mass determination, we refer to these error estimates as "systematic errors". We stress, however, that these errors do not include the error introduced by the quenched approximation.

For plots with the pion mass squared on the horizontal axis, we use a specific combination of Gaussian interpolators for extracting the ground state pion mass. The corresponding statistical error gives rise to the horizontal error bars in some of our plots which are, however, smaller than the symbols used.

When fitting eigenvalues obtained with the variational method we experimented with both correlated and uncorrelated (two-parameter) exponential fits. For the correlated fits we used a jackknife estimate of the correlation matrix which was not always stable with our ensemble of configurations. For the generation of the plots we therefore resorted to simple uncorrelated fits throughout, using only the diagonal elements of the covariance matrix. For the cases, where correlated fits are stable and a direct comparison with uncorrelated fits is possible, we find that the latter give larger statistical errors [39]. This explains the rather small χ^2/d.o.f. we find. Thus the uncorrelated errors we give in the plots and in the Appendix (Tables II, III, IV, V, VI, VII, VIII, IX, and X) are probably overestimated.

E. A first look at the derivative sources

Figure 1 shows the diagonal elements of the correlation matrix for some of the channels considered. Compared to the interpolators from Reference [9] (without derivative sources), the interpolators with derivative sources show stronger contributions from excited states, i.e., they have a steeper slope for small Euclidean time t. Nevertheless, for all interpolators the ground state in the respective channel dominates the behavior at large time separation, i.e., all correlators in Fig. 1 display the same slope at sufficiently large t.

We remark that the propagators in the 0^{++} channel at the lightest quark masses show a deviation from that pattern for small t due to ghosts. A more detailed discussion of the scalar correlators will be given in Sec. III B.

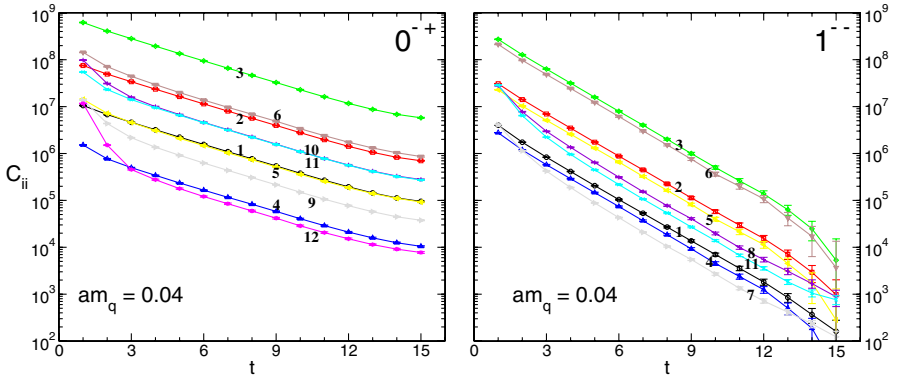

FIG. 1 (color online). Diagonal entries of the correlation matrix as a function of t. The data are for bare quark mass $am_q = 0.04$. The 0^{-+} (left-hand side plot) and 1^{--} (right-hand side) channels are shown. The numbers next to the correlators are according to Table I.

As suggested by Fig. 1, the pion ground state can be fitted from a single diagonal correlator at all quark masses. Stable plateaus are obtained in the time interval $t = 6 \ldots 15$ where cosh fits can be performed for the individual correlators. For the lowest quark mass $am_q = 0.02$ the statistical error usually is of the order of 1–2% of the fitted value with the derivative sources leading to a somewhat larger error. An exception is interpolator 12 where the statistical error is about 3.5% of the fitted value. At larger masses the error is substantially smaller. The fit values for the ground state pion mass from the different individual correlators, shown in the left-hand side plot of Fig. 1, agree within two sigma. For the 1^{--} channel similar observations hold.

F. Contributions from backward propagation

In Fig. 2 we show the three largest eigenvalues obtained from the generalized problem (3) for the pion case. It is obvious that on the logarithmic scale used in this plot the three eigenvalues give rise to three essentially straight lines for sufficiently small t. The different slopes correspond to the masses of the ground, first and second excited states.

For mesons, forward and backward propagation behaves in the same way. Each interpolator coupling to a particular state at early times will also couple to the same, but backward running, state at later time. Higher channels in the generalized eigenvalue problem may in this way turn into lighter state signals. This interesting observation (see also [40]), particular to the generalized eigenvalue problem, can be made for the second eigenvalue in Fig. 2: At $t \sim 9$ (when using $t_0 = 1$) the data points of the second eigenvalue change their behavior and start to increase again. Beyond $t = 9$ the data points form a straight line with positive slope. This upward pointing straight line turns around again at $t \sim 13$ and from there on decays with a slope corresponding to the ground state mass. Also the slope of the upwards pointing piece between $t = 9$ and $t = 13$ (which is then continued by an upward pointing piece of the largest eigenvalue), has the slope of the ground state mass.

This avoided level crossing scenario has an important consequence: The generalized eigenvalue problem disentangles the forward propagating ground and excited state masses only up to the first crossing with the backward running lightest propagator, which for our example happens at $t \sim 9$. Beyond that value also the second eigenvalue, which for small t is dominated by the first excitation, couples to the lighter ground state (running "backwards") and no longer provides information on the excitations. In particular in the 0^{-+} channel, where a backward running light pion crosses with the second eigenvalue already at a small t, this effect limits the analysis of excited states [41].

The comments of this subsection are particularly important for light pseudoscalars. For the pions it is the backward running contributions that limit the fit range with the

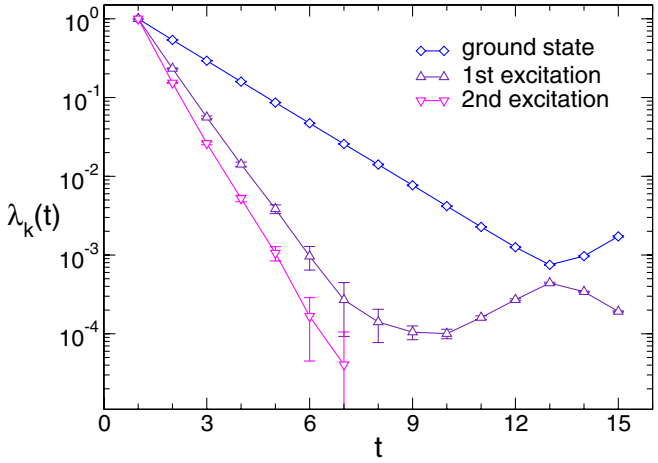

FIG. 2 (color online). First three eigenvalues from the generalized eigenproblem (3) for the 0^{-+} channel as a function of t.

generalized eigenproblem, leading to errors comparable with the errors obtained from fitting single correlators with the correct functional form.

III. RESULTS FOR INDIVIDUAL MESON CHANNELS

A. The 0^{-+} channel

Figure 3 shows the results for the first excited state of the pion. We display the results for two different sets of interpolators. Circles are used for the combination of Gaussian interpolators 1, 4, 5, 6, while the squares correspond to the combination 1, 4, 6, 9, 12 of Gaussian and derivative interpolators. While combinations of Gaussian and derivative interpolators allow for fits at slightly lighter quark masses, the interpolators with derivative sources couple weaker to the ground state. The systematical uncertainty (shaded region in the figure) from the choice of interpolators is consistent with statistical effects as reasonable combinations of four or more interpolators lie within one sigma of our final fit result. While there is no significant improvement, the new results with a larger basis nicely confirm the existence of the measured state.

With a combination of Gaussian and derivative interpolators, it is also possible to obtain fits for a second excited state which could not be observed before. This state is displayed in Fig. 4. In the chiral limit, this state can most likely be identified with the $\pi(1800)$. Fits with various different combinations of interpolators lead to the same results which all show stable eigenvector entries.

It is instructive to look at the components of the eigenvectors for all three states observed in the pseudoscalar channel. Figure 5 shows such a plot. While the derivative interpolators 9 and 10 do not contribute significantly to the ground and first excited states, they are most important for obtaining the newly observed second excited state. This behavior is qualitatively the same for all possible combinations of interpolators where the second excited state could be seen.

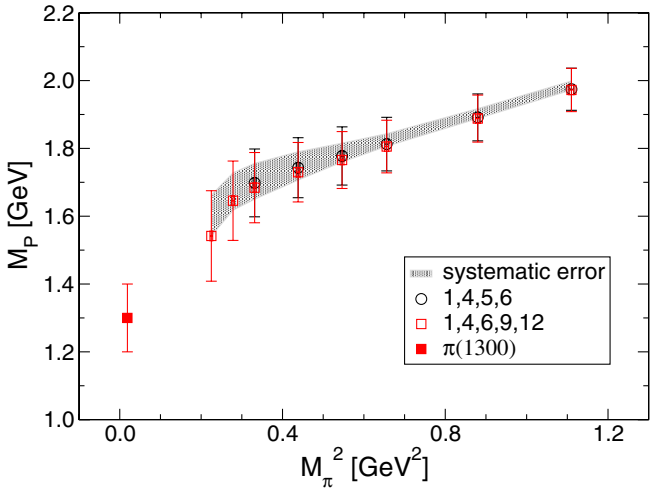

FIG. 3 (color online). First excited state of the pseudoscalars for two different sets of interpolators. The error bars are statistical only and the shaded region indicates the additional systematic error as discussed. The filled symbol corresponds to the experimentally measured $\pi(1300)$.

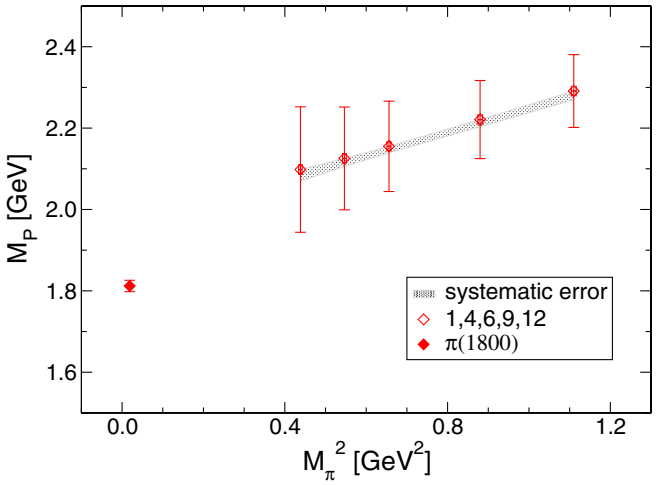

FIG. 4 (color online). Second excited state for the pseudoscalars. The filled symbol indicates the $\pi(1800)$.

While the reduction in the statistical error for the first excited state can merely be attributed to an enlargement of the basis, the second excited state is only observed when including derivative interpolators. We would like to stress that a correlation matrix of similar size consisting solely of nonderivative operators does not enable us to see this excitation.

B. The 0^{++} channel

In the 0^{++} channel contributions from ghosts [26,27,42–45], arising from the $\eta'\pi$ contribution to the isovector-scalar correlators, are expected and must be identified for a clean interpretation of the data. These unphysical contributions due to quenching have a negative spectral weight and dominate the correlators at small quark masses, leading to correlators which become negative at intermediate time separations. Figure 6 shows the diagonal correlators for the scalar channel at our smallest quark mass $am_q = 0.02$. While some of them (1–3) display a very prominent ghost contribution, others show a much smaller contribution. Correlators 7 and 8 feel no effects from ghosts at all with our limited statistics, which may be related to their different chiral structure (see Table I). We note that these two interpolators do not seem to couple in the dynamical case, as our preliminary dynamical results do not show a signal for these correlators.

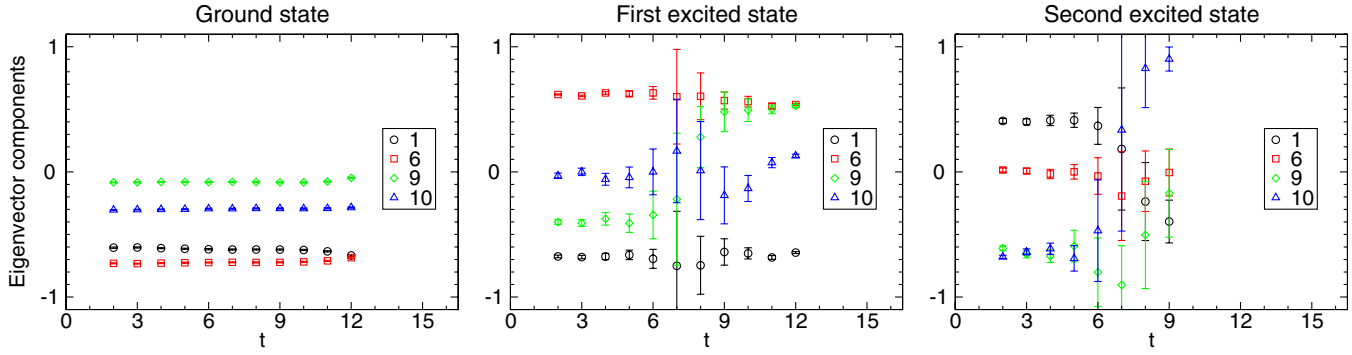

FIG. 5 (color online). Eigenvector components from the standard eigenvalue problem (6) as a function of t. The eigenvectors correspond to the pion ground state (left-hand side plot), the first and second excited states (center and right-hand side plots) and are obtained from a 4×4 matrix of the interpolators 1, 6, 9, 10, at quark mass $am_q = 0.12$.

While the variational approach enables us to disentangle most of these ghost contributions [27], at low quark masses the quality of the observed plateaus quickly deteriorates for the Gaussian interpolators leading to large error bars for the a_0 ground state.

The additional interpolators with derivative sources enlarge the correlation matrix, which is vital in the presence of ghost contributions. Furthermore, it is these interpolators which couple only weakly to the ghosts. Using the variational method we are able to disentangle the leading ghost contribution and in some cases even a subleading ghost contribution, corresponding to a $\eta'\pi$ state with relative momentum.

Figure 7 shows the results for the largest eigenvalue of the variational analysis. The plot demonstrates that derivative sources enable us to perform fits at smaller quark masses with reduced statistical errors in the intermediate and heavy quark mass region.

The shaded region in Fig. 7 indicates our estimate of the additional systematic errors due to the choice of fit ranges and interpolators considered. As it remains unclear which systematics cause the dependence on the choice of interpolators in this channel, we refrain from an extrapolation to the physical mass region. Interpolators with strong ghost contributions, however, tend to lead to higher mass values suggesting the ground state to be in the region of the $a_0(1450)$, while a fit with those interpolators containing no visible ghost contribution leads to values in the lower parts of the shaded region.

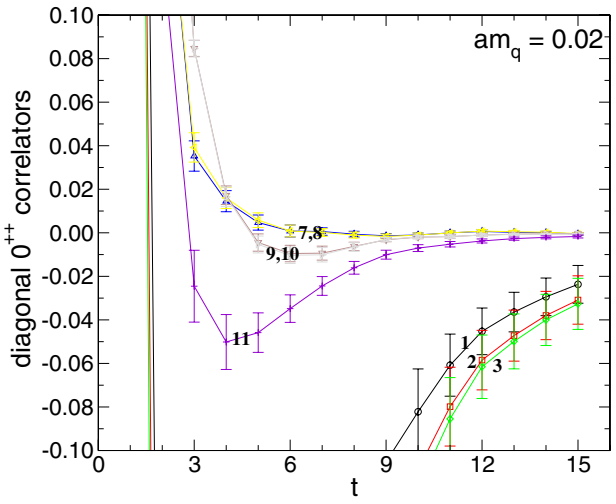

FIG. 6 (color online). Diagonal entries of the correlation matrix for the scalar channel at $am_q = 0.02$. The numbers next to the data label the correlators according to Table I. There are clear contributions of ghost states for some interpolators (i.e., negative values), while other interpolators seem to be almost free of them.

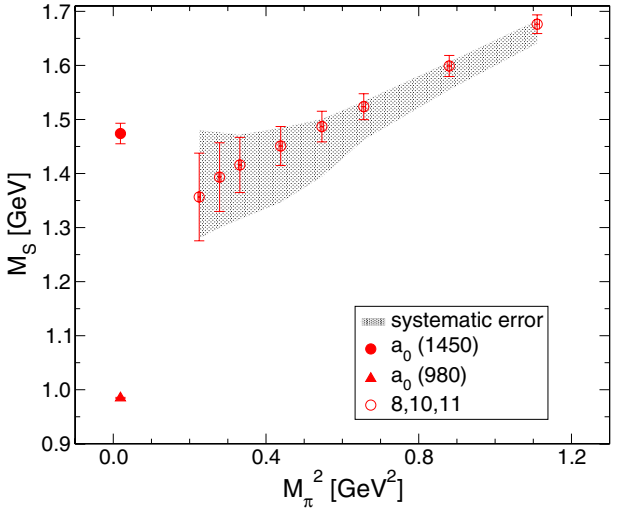

FIG. 7 (color online). Ground state mass of the isovector scalar (a_0). The error bars are statistical only and the shaded region indicates the additional systematic error described in the text. The black circle shows the (experimentally) measured $a_0(1450)$ and the triangle indicates the $a_0(980)$.

For this channel large quenching effects might influence the result. Thus it is not clear whether the data should extrapolate to the $a_0(980)$ or the $a_0(1450)$. More light will be shed on this channel only when dynamical data are available where no quenched ghosts are present [46]. If the systematic deviations we observe in the choice of interpolators are due to ghosts, one should expect the results to become more consistent with dynamical data.

A review of issues faced in the scalar channel and a detailed discussion of the possible nature of the isovector-scalar ground state can be found in the recent review by McNeile [47].

C. The 1^{--} channel

As mentioned before, the ground state for the vector meson, the $\rho(770)$, can also be fit from single correlators. However the results improve quite drastically when a matrix of interpolators is used.

Figure 8 shows the 1^{--} meson ground state and illustrates the good quality of the data in the quenched approximation, where no decay is possible. The results from different interpolators and fit ranges agree within error bars.

The interpretation for the first and second excitation in the 1^{--} channel is less clear. From experiment we know of multiple excitations with $J = 1$ below 2 GeV, the most established being the $\rho(1450)$ and the $\rho(1700)$. In addition, due to loss of continuous Lorentz symmetry, some of the lattice interpolators we chose may in principle couple to continuum states with higher J [14,18], and there is at least one such excitation known in the vector channel, the $\rho_3(1690)$. Excluding this possibility would be a difficult task which might be overcome by taking a look at different irreducible representations of the hypercubic group where degeneracy of states in different representations can be used to identify the correct J, as has been demonstrated for baryons [19–21].

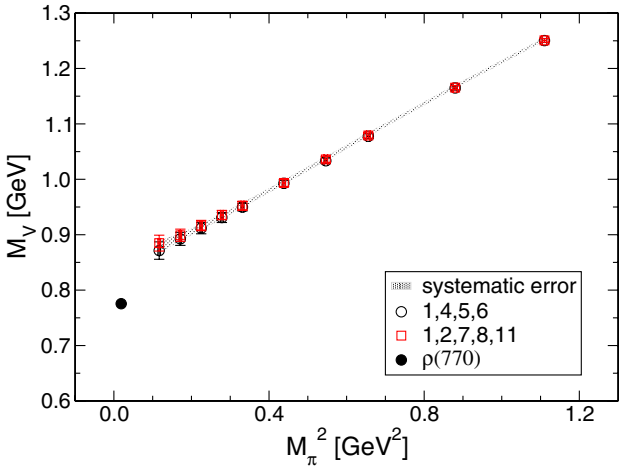

FIG. 8 (color online). Ground state for the $\rho(770)$ meson.

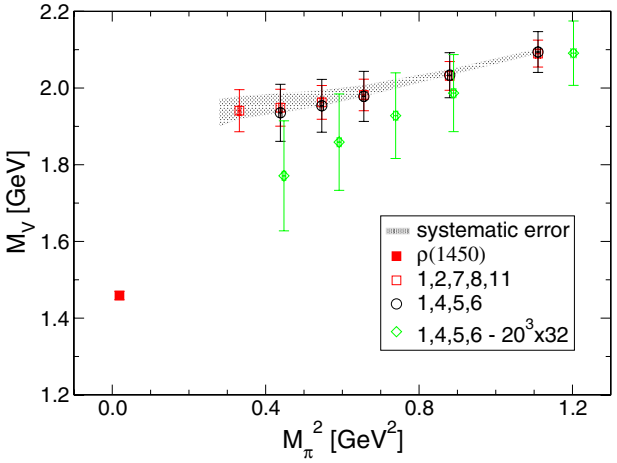

FIG. 9 (color online). First excited state for the ρ meson, compared to the first experimental meson resonance with $J = 1$, the $\rho(1450)$. The diamonds represent an alternative fit of data from [9] for a finer lattice of the same volume ($20^3 \times 32$, $a = 0.119$ fm).

As can be seen in Figs. 9 and 10, the values obtained from combinations of Gaussian interpolators agree qualitatively with the values obtained from the larger basis, while the larger basis leads to overall smaller error bars and somewhat more stable plateaus. Nevertheless, the two excitations are too close together and would both be consistent with the $\rho(1700)$. This problem has already been encountered in [19], where both the $16^3 \times 32$ lattice with spacing $a = 0.148$ fm, and a finer $20^3 \times 32$ lattice with $a = 0.119$ fm have been used. The data from the fine lattice lead to two distinct excitations

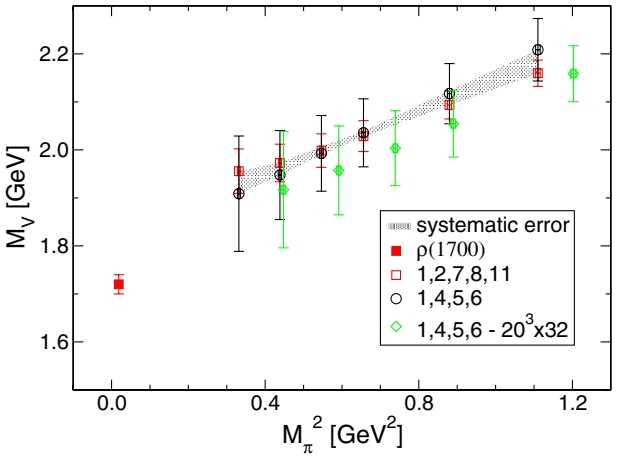

FIG. 10 (color online). Second excitation in the vector channel compared to the $\rho(1700)$. Again the diamonds indicate data from the finer lattice.

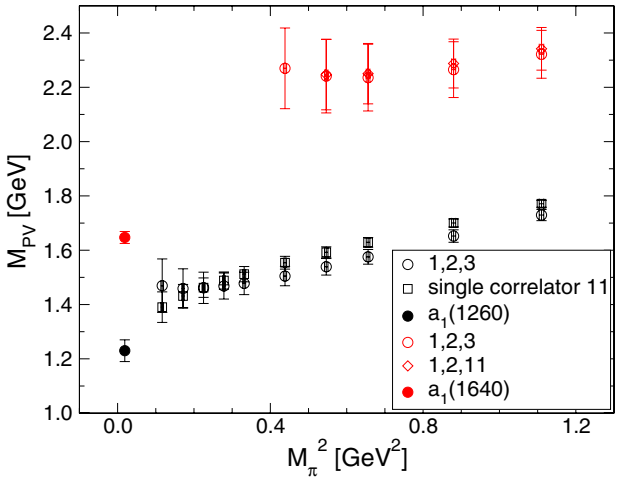

FIG. 11 (color online). Ground and first excited state of the pseudovector mesons (a_1). The filled circles indicate the physical states.

compatible with an interpretation as the physical $\rho(1450)$ and $\rho(1700)$. To demonstrate this, we also included an alternative fit of the old data from the fine lattice in Figs. 9 and 10.

Inspecting the eigenvectors of the states, we can identify them by their operator content and come to the conclusion that they are indeed the same on both lattices. Moreover, as both lattices have the same physical volume, this leads us to an interpretation of the difference as a discretization effect. Such an explanation seems reasonable as the states are rather close to each other. We therefore are confident that the method works and that the same calculation on finer lattices would lead to results in better agreement with experiment.

D. The 1^{++} channel

For the 1^{++} channel, there is only one interpolator containing derivative quark sources. Figure 11 shows data obtained from different combinations of Gaussian interpolators and the one containing derivatives. An indication of error bands, as shown for the other channels, has been omitted here, since the two combinations plotted already show the extremes.

Figure 11 demonstrates a clear improvement in the description of the ground state using the interpolator with derivative quark sources. While the results from the Gaussian and the full sets agree qualitatively, the statistical errors towards smaller quark masses are significantly reduced. The reason for this is the longer, more stable effective mass plateaus allowing for larger fit ranges. At larger quark masses there is a slight deviation of the order of 2 sigma.

The excited state previously observed stays the same if one includes the new interpolator in the analysis. Looking at the components of the modified eigenvalue problem we see that this interpolator contributes only weakly to this excited state.

IV. SUMMARY

In this article we have explored the impact of derivative sources in light meson spectroscopy. The sources are obtained by applying a covariant derivative on a Jacobi-smeared quark source. Interpolators based on derivative sources were tested in a quenched excited meson spectroscopy calculation based on the variational method.

We find that both ground and excited state signals may be improved, depending on the channel. For the 0^{-+} channel we find that the quality of the first excited state improves and fits become possible for smaller quark masses. In addition a second excited state can be identified when adding interpolators with derivative sources in the correlation matrix.

The 0^{++} channel is dominated by the presence of ghosts at small quark masses which we essentially disentangle using the variational method. The additional interpolators with derivative sources are helpful since they enlarge the correlation matrix and some of them couple only very weakly to the ghost states. They allow one to fit scalar masses at lower quark masses, although the results still depend significantly on the choice of interpolators used in the correlation matrix. This indicates that results for this channel from a quenched calculation should be interpreted only with the necessary caution.

For the 1^{--} mesons we demonstrate that the inclusion of derivative sources leads to results with a smaller statistical error which agree excellently with the results published before.

For the 1^{++} channel we show that the derivative sources drastically improve the signal for the ground state. At the same time a matrix of interpolators enables us to identify a second excited state.

ACKNOWLEDGMENTS

We thank Tommy Burch, Julia Danzer and Markus Limmer for discussions. D. M. and L. Ya. G. acknowledge support by "Fond zur Förderung der wissenschaftlichen Forschung in Österreich" (FWF DK W1203-N08 and P19168-N16). The data were generated on computers at the Leibniz Rechenzentrum, Garching, Germany and at the ZID, Graz, Austria.

APPENDIX: TABLES OF MASSES

The tables in this Appendix collect our results for the masses in the various meson channels we analyzed for various values of the quark mass parameter and different choices of the interpolator set. We furthermore provide the statistical errors and the corresponding χ^2/d.o.f., as well as the fit ranges that were used.

TABLE II. Ground state in the 0^{-+} channel (pion).

Interpolators	m_q	Mass [GeV]	Error	Fit range	χ^2/d.o.f.
1,4,5,6	0.20	1.0535	0.0025	4–10	0.09
	0.16	0.9379	0.0025	4–10	0.11
	0.12	0.8098	0.0026	4–10	0.13
	0.10	0.7391	0.0027	4–10	0.14
	0.08	0.6621	0.0028	4–10	0.14
	0.06	0.5759	0.0029	4–10	0.14
	0.05	0.5279	0.0029	4–10	0.13
	0.04	0.4750	0.0030	4–10	0.12
	0.03	0.4151	0.0032	4–10	0.12
	0.02	0.3420	0.0039	4–10	0.13
1,6,9,10	0.20	1.0536	0.0029	3–9	0.10
	0.16	0.9380	0.0029	3–9	0.12
	0.12	0.8100	0.0030	3–9	0.17
	0.10	0.7392	0.0031	3–9	0.20
	0.08	0.6621	0.0032	3–9	0.25
	0.06	0.5757	0.0033	3–9	0.29
	0.05	0.5274	0.0034	3–9	0.32
	0.04	0.4742	0.0036	3–9	0.35
	0.03	0.4136	0.0039	3–9	0.40
	0.02	0.3414	0.0052	3–9	0.49
1,4,6,9,12	0.20	1.0534	0.0023	3–9	0.10
	0.16	0.9377	0.0024	3–9	0.13
	0.12	0.8096	0.0024	3–9	0.17
	0.10	0.7390	0.0028	3–9	0.20
	0.08	0.6619	0.0028	3–9	0.24
	0.06	0.5755	0.0029	3–9	0.28
	0.05	0.5271	0.0030	3–9	0.30
	0.04	0.4744	0.0036	3–9	0.33
	0.03	0.4140	0.0039	3–9	0.38
	0.02	0.3418	0.0050	3–9	0.48

TABLE III. First excited state in the 0^{-+} channel.

Interpolators	m_q	Mass [GeV]	Error	Fit range	χ^2/d.o.f.
1,4,5,6	0.20	1.974	0.062	3–7	0.10
	0.16	1.891	0.069	3–7	0.09
	0.12	1.813	0.079	3–7	0.04
	0.10	1.778	0.086	3–7	0.02
	0.08	1.743	0.088	3–6	0.01
	0.06	1.698	0.100	3–6	0.02
1,6,9,10	0.20	1.999	0.047	3–7	0.02
	0.16	1.917	0.054	3–7	0.01
	0.12	1.834	0.062	3–6	0.07
	0.10	1.791	0.070	3–6	0.14
	0.08	1.744	0.082	3–6	0.21
	0.06	1.675	0.101	3–6	0.15
	0.05	1.618	0.116	3–6	0.05
1,4,6,9,12	0.20	1.972	0.064	3–7	0.11
	0.16	1.888	0.069	3–7	0.10
	0.12	1.805	0.078	3–7	0.03
	0.10	1.766	0.084	3–7	0.05
	0.08	1.730	0.088	3–6	0.06
	0.06	1.684	0.104	3–6	0.03
	0.05	1.646	0.117	3–6	0.07
	0.04	1.542	0.133	3–6	0.04

TABLE IV. Second excited state in the 0^{-+} channel.

Interpolators	m_q	Mass [GeV]	Error	Fit range	χ^2/d.o.f.
1,6,9,10	0.20	2.266	0.108	3–7	0.01
	0.16	2.199	0.109	3–7	0.02
	0.12	2.142	0.120	3–6	0.07
	0.10	2.113	0.134	3–6	0.12
	0.08	2.082	0.162	3–6	0.14
1,4,6,9,12	0.20	2.291	0.089	3–6	0.08
	0.16	2.221	0.096	3–6	0.08
	0.12	2.155	0.111	3–6	0.06
	0.10	2.125	0.126	3–6	0.04
	0.08	2.098	0.154	3–6	0.01

TABLE V. Ground state in the 0^{++} channel.

Interpolators	m_q	Mass [GeV]	Error	Fit range	χ^2/d.o.f.
8,10,11	0.20	1.676	0.017	4–7	0.07
	0.16	1.599	0.019	4–7	0.14
	0.12	1.524	0.024	4–7	0.28
	0.10	1.487	0.028	4–7	0.37
	0.08	1.451	0.036	4–7	0.41
	0.06	1.416	0.051	4–7	0.34
	0.05	1.393	0.064	4–7	0.24
	0.04	1.357	0.081	4–7	0.15

TABLE VI. Ground state in the 1^{--} channel.

Interpolators	m_q	Mass [GeV]	Error	Fit range	χ^2/d.o.f.
1,4,5,6	0.20	1.251	0.0041	3–9	0.01
	0.16	1.165	0.004	3–9	0.01
	0.12	1.079	0.005	3–9	0.01
	0.10	1.036	0.005	3–9	0.01
	0.08	0.993	0.006	3–9	0.01
	0.06	0.950	0.007	3–9	0.02
	0.05	0.931	0.009	3–6	0.01
	0.04	0.912	0.010	3–6	0.01
	0.03	0.893	0.012	3–6	0.02
	0.02	0.871	0.016	3–6	0.06
1,2,7,8,11	0.20	1.251	0.003	3–12	0.02
	0.16	1.165	0.004	3–12	0.04
	0.12	1.079	0.005	3–12	0.06
	0.10	1.036	0.005	3–12	0.07
	0.08	0.993	0.006	3–12	0.07
	0.06	0.952	0.008	3–12	0.06
	0.05	0.933	0.009	3–12	0.04
	0.04	0.914	0.011	3–12	0.03
	0.03	0.896	0.013	3–12	0.02
	0.02	0.881	0.017	3–12	0.07

TABLE VII. First excited state in the 1^{--} channel.

Interpolators	m_q	Mass [GeV]	Error	Fit range	χ^2/d.o.f.
1,4,5,6	0.20	2.094	0.053	3–6	0.05
	0.16	2.033	0.059	3–6	0.06
	0.12	1.978	0.065	3–6	0.06
	0.10	1.954	0.069	3–6	0.05
	0.08	1.935	0.074	3–6	0.04
1,2,7,8,11	0.20	2.091	0.037	3–7	0.05
	0.16	2.033	0.040	3–7	0.06
	0.12	1.985	0.044	3–7	0.11
	0.10	1.968	0.046	3–7	0.16
	0.08	1.957	0.049	3–7	0.21
	0.06	1.941	0.055	3–6	0.14

TABLE VIII. Second excited state in the 1^{--} channel.

Interpolators	m_q	Mass [GeV]	Error	Fit range	χ^2/d.o.f.
1,4,5,6	0.20	2.209	0.065	3–6	1.49
	0.16	2.117	0.063	3–6	1.50
	0.12	2.036	0.071	3–6	0.98
	0.10	1.993	0.079	3–6	0.62
	0.08	1.948	0.093	3–6	0.25
	0.06	1.909	0.120	3–6	0.08
1,2,7,8,11	0.20	2.178	0.029	3–7	1.25
	0.16	2.111	0.030	3–7	1.18
	0.12	2.031	0.031	3–7	0.42
	0.10	2.000	0.034	3–7	0.33
	0.08	1.974	0.038	3–7	0.24
	0.06	1.956	0.046	3–6	0.21

TABLE IX. Ground state in the 1^{++} channel.

Interpolators	m_q	Mass [GeV]	Error	Fit range	χ^2/d.o.f.
1,2,3	0.20	1.729	0.021	3–7	0.55
	0.16	1.652	0.023	3–7	0.47
	0.12	1.576	0.027	3–7	0.36
	0.10	1.539	0.031	3–7	0.30
	0.08	1.505	0.036	3–7	0.23
	0.06	1.478	0.041	3–6	0.26
	0.05	1.468	0.048	3–6	0.20
	0.04	1.461	0.058	3–6	0.13
	0.03	1.459	0.073	3–6	0.06
	0.02	1.469	0.099	3–6	0.02
11	0.20	1.771	0.013	4–9	0.19
	0.16	1.700	0.015	4–9	0.26
	0.12	1.629	0.018	4–9	0.34
	0.10	1.592	0.020	4–9	0.34
	0.08	1.554	0.023	4–9	0.29
	0.06	1.512	0.028	4–9	0.16
	0.05	1.488	0.031	4–9	0.08
	0.04	1.462	0.036	4–9	0.04
	0.03	1.432	0.043	4–9	0.16
	0.02	1.390	0.056	4–9	0.76

TABLE X. First excited state in the 1^{++} channel.

Interpolators	m_q	Mass [GeV]	Error	Fit range	χ^2/d.o.f.
1,2,3	0.20	2.322	0.088	3–6	0.06
	0.16	2.265	0.103	3–6	0.04
	0.12	2.236	0.123	3–6	0.02
	0.10	2.241	0.136	3–6	0.03
	0.08	2.270	0.149	3–6	0.09
1,2,11	0.20	2.342	0.079	3–6	0.01
	0.16	2.288	0.090	3–6	0.02
	0.12	2.250	0.111	3–6	0.04
	0.10	2.247	0.130	3–6	0.07

[1] M. Asakawa, T. Hatsuda, and Y. Nakahara, Prog. Part. Nucl. Phys. **46**, 459 (2001).
[2] G. Lepage *et al.*, Nucl. Phys. B, Proc. Suppl. **106**, 12 (2002).
[3] Y. Chen *et al.*, arXiv:hep-lat/0405001.
[4] G. T. Fleming, arXiv:hep-lat/0403023.
[5] H.-W. Lin and S. D. Cohen, arXiv:0709.1902.
[6] G. M. von Hippel, R. Lewis, and R. G. Petry, Proc. Sci., LAT2007 (2007) 043 [arXiv:0710.0014].
[7] C. Michael, Nucl. Phys. **B259**, 58 (1985).
[8] M. Lüscher and U. Wolff, Nucl. Phys. **B339**, 222 (1990).
[9] T. Burch *et al.*, Phys. Rev. D **73**, 094505 (2006).
[10] T. Burch *et al.*, Phys. Rev. D **74**, 014504 (2006).
[11] T. Burch *et al.*, Nucl. Phys. **A755**, 481 (2005).
[12] T. Burch *et al.* (Bern-Graz-Regensburg Collaboration), Phys. Rev. D **70**, 054502 (2004).
[13] X. Liao and T. Manke, arXiv:hep-lat/0210030.
[14] J. J. Dudek, R. G. Edwards, N. Mathur, and D. G. Richards, Phys. Rev. D **77**, 034501 (2008).
[15] M. Wingate, T. A. DeGrand, S. Collins, and U. M. Heller, Phys. Rev. Lett. **74**, 4596 (1995).
[16] T. Burch, C. Hagen, and A. Schäfer, Proc. Sci. LAT2006 (2006) 177 [arXiv:hep-lat/0609014].
[17] T. Burch, C. Ehmann, C. Hagen, M. Hetzenegger, and A. Schäfer, Proc. Sci. LATTICE2007 (2007) 103 [arXiv:0709.0664].
[18] P. Lacock, C. Michael, P. Boyle, and P. Rowland (UKQCD Collaboration), Phys. Rev. D **54**, 6997 (1996).
[19] S. Basak *et al.* (Lattice Hadron Physics (LHPC) Collaboration), Phys. Rev. D **72**, 074501 (2005).
[20] S. Basak *et al.*, Phys. Rev. D **72**, 094506 (2005).
[21] S. Basak *et al.*, Phys. Rev. D **76**, 074504 (2007).
[22] S. Basak *et al.*, arXiv:hep-lat/0609052.
[23] C. Gattringer, L. Y. Glozman, C. B. Lang, D. Mohler, and S. Prelovsek, Proc. Sci. LAT2007 (2007) 123 [arXiv:0709.4456].
[24] C. Gattringer, arXiv:0711.0622 [Eur. Phys. J. A (to be published)].
[25] C. B. Lang, Prog. Part. Nucl. Phys. **61**, 35 (2008).
[26] W. A. Bardeen, A. Duncan, E. Eichten, N. Isgur, and H. Thacker, Phys. Rev. D **65**, 014509 (2001).
[27] T. Burch, C. Gattringer, L. Y. Glozman, C. Hagen, and C. B. Lang, Phys. Rev. D **73**, 017502 (2006).
[28] S. Güsken *et al.*, Phys. Lett. B **227**, 266 (1989).
[29] C. Best *et al.*, Phys. Rev. D **56**, 2743 (1997).
[30] Notice that interpolators with covariant derivatives may receive additional terms in their chiral representation.
[31] L. Y. Glozman, Phys. Lett. B **587**, 69 (2004).
[32] L. Y. Glozman, Phys. Rep. **444**, 1 (2007).
[33] L. Y. Glozman and A. V. Nefediev, Phys. Rev. D **76**, 096004 (2007).
[34] M. Lüscher and P. Weisz, Commun. Math. Phys. **97**, 59 (1985); **98**, 433(E) (1985).
[35] G. Curci, P. Menotti, and G. Paffuti, Phys. Lett. **130B**, 205 (1983); **135B**, 516(E) (1984).
[36] C. Gattringer, R. Hoffmann, and S. Schaefer, Phys. Rev. D **65**, 094503 (2002).
[37] C. Gattringer, Phys. Rev. D **63**, 114501 (2001).
[38] C. Gattringer, I. Hip, and C. B. Lang, Nucl. Phys. **B597**, 451 (2001).
[39] C. Gattringer *et al.* (Bern-Graz-Regensburg Collaboration), Nucl. Phys. **B677**, 3 (2004).
[40] A. C. Lichtl, Proc. Sci. LAT2007 (2007) 118 [arXiv:0711.4072].
[41] We remark, however, that in a 2-d pilot study, where very accurate data can be obtained, we found that after the first crossing the third eigenvalue takes over the slope of the first excitation. Thus it seems possible to extract additional information on the first excitation from higher eigenvalues.
[42] W. A. Bardeen, E. Eichten, and H. Thacker, Phys. Rev. D **69**, 054502 (2004).
[43] S. Prelovsek and K. Orginos (RBC Collaboration), Nucl. Phys. B, Proc. Suppl. **119**, 822 (2003).
[44] S. Prelovsek, C. Dawson, T. Izubuchi, K. Orginos, and A. Soni, Phys. Rev. D **70**, 094503 (2004).
[45] N. Mathur *et al.*, Phys. Rev. D **76**, 114505 (2007).
[46] R. Frigori *et al.*, Proc. Sci. LAT2007 (2007) 114 [arXiv:0709.4582].
[47] C. McNeile, Proc. Sci. LATTICE2007 (2007) 019 [arXiv:0710.0985].